

THE GENERATING CONDITIONS OF A HIGH-REYNOLDS-NUMBER SWIRLING JET

Benjamin Leclaire, Laurent Jacquin and Denis Sipp
ONERA/DAFE
8 rue des Vertugadins, 91290 Meudon, France
benjamin.leclaire@onera.fr

ABSTRACT

We study experimentally the dynamics of the duct flow upstream of a high-Reynolds number swirling jet. Our setup involves a rotating honeycomb and allows to vary the contraction ratio of the final duct portion preceding the jet exhaust plane. Stereo-PIV measurements are realized in the duct directly upstream of these final portions, for increasing values of the swirl number. It is shown that the flow dynamics is strongly influenced by its supercritical or subcritical nature with respect to axisymmetric inertial waves. In the subcritical regime, complex mean flows are observed, which differ according to the duct geometry under consideration. Discrepancies are in turn detected in the flow unsteady behaviour, with the appearance, at the highest values of the swirl number, of transient small-scale recirculations located either close to the duct axis or near the edge of the boundary layer.

INTRODUCTION

Swirling jet experiments are designed to produce a radially unconfined flow with both an axial and an azimuthal component of velocity. They traditionally involve a rotation-imparting device such as swirl vanes or a rotating honeycomb, followed by cylindrical duct portions in which the flow is settled or accelerated before exhausting as a free jet. Past experiments dealing with such configurations have chosen the exit plane flow as their upstream boundary condition, and aimed at establishing links between the velocity profile there and the subsequent dynamics of the jet (see e.g. Panda and McLaughlin, 1994, and Billant et al. 1998). Such an approach has allowed significant progress in the understanding of phenomena specific of rotating flows, e.g. centrifugal instabilities, modified properties of the turbulence and of the jet potential cone, and vortex breakdown.

In our high-Reynolds-number swirling jet facility, a uniformly rotating flow is generated by a rotating honeycomb, and passes through a portion of constant cross-section duct terminated or not by a converging portion. In some regimes, fully turbulent flow has been measured in the exit plane, thereby suggesting that the duct flow could blur the generating condition of the jet. To our knowledge, no detailed account exists in the literature on the dynamics of the duct flow preceding swirling jets. We thus investigated the flow directly upstream from the final duct portion by means of Stereoscopic PIV, with respect to both the swirl number of the flow exiting from the honeycomb and the final contraction ratio. This paper presents the outcome of this work, and is organized as follows. The experimental setup is first described. In a second part, mean flow quantities are analyzed in order to define several flow regimes, controlled by the value of the swirl number. The unsteady dynamics of the flow is then analyzed for some of these regimes.

EXPERIMENTAL SETUP

We use a centrifugal fan to generate an axial flow in a cylindrical duct of radius R_0 . This radius is taken as the reference length throughout the study. We also use a cylindrical coordinate basis (r, θ, z) and denote the corresponding instantaneous velocity components as (u, v, w) . The mean and fluctuating velocity components will be respectively denoted as (U, V, W) and (u', v', w') . As sketched in figure 1, rotation is imparted to the initially axial flow by means of a rotating duct portion equipped with a fine-celled honeycomb. For moderate values of the angular velocity Ω_0 , the flow has a uniform axial velocity and rotates as a rigid body except in the boundary layers. It develops in a duct of constant cross-section, whose downstream part is transparent in order to allow Stereo-PIV measurements in a longitudinal plane. The measurement zone is represented by a shaded rectangle in figure 1. The flow is then accelerated by a converging duct and finally exhausts as a swirling jet.

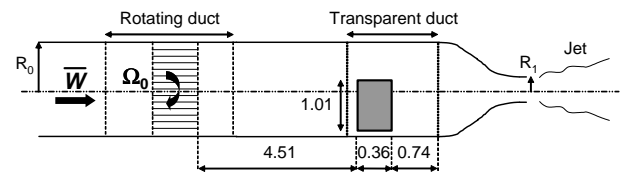


Figure 1: Schematic description of the wind-tunnel. The flow zone investigated by S-PIV is shaded. Lengths are nondimensionalized using the upstream duct radius R_0 . \bar{W} denotes the mean axial velocity built from the volume flow rate.

The contraction ratio of the final duct portion is defined as

$$\chi_{CV} = (R_0/R_1)^2 \quad (1)$$

where R_1 stands for its downstream radius. We consider four different duct geometries, $\chi_{CV} = 1$ (i.e. with a constant cross-section), 4, 9 and 18.4. The second variable control parameter is the swirl number S of the flow exiting from the honeycomb,

$$S = \frac{R_0 \Omega_0}{\bar{W}}, \quad (2)$$

where \bar{W} denotes the mean axial velocity built from the volume flow rate. For each of the duct geometries, S is varied from 0 to about 3.4 by first setting the plug axial velocity of the flow when $\Omega_0 = 0$, and subsequently increasing Ω_0 by small steps. At each step, 800 images are recorded at a frequency $f_a = 4 \text{ Hz}$.

The Reynolds number of the flow is defined by $Re = 2R_0 \bar{W} / \nu$. It is comprised between 55100 and 58100 for $\chi_{CV} = 4, 9$ and 18.4, and between 50500 and 56700 for $\chi_{CV} = 1$.

FLOW REGIMES

Figure 2 shows the mean axial velocity W , nondimensionalized by \bar{W} , measured at the centre of the duct, $r = 0$, at the axial location $z = 4.70$. It should be noted here that in the following, all plotted quantities will be extracted from this precise axial location unless otherwise stated.

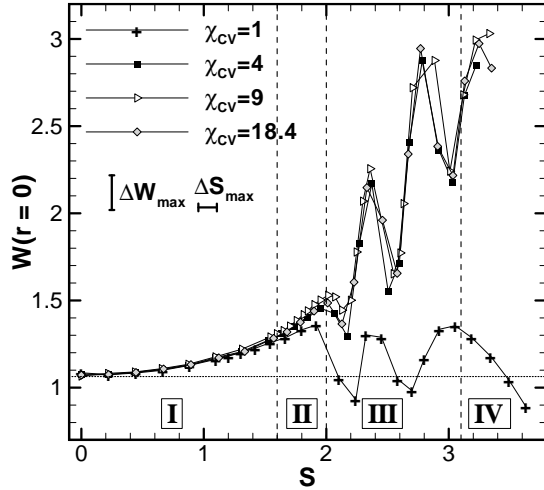


Figure 2: Mean axial velocity W at $r = 0$, $z = 4.70$, as a function of S , for the different contraction ratios χ_{CV} . The horizontal dotted line separates flow with a velocity excess on the axis from flows with a velocity defect on the axis.

As the honeycomb is set into motion (increasing S), the axial velocity profile progressively departs from uniformity. As a matter of fact, $W(r = 0)$ gradually increases i.e. the profile of W becomes parabolic with a velocity excess on the axis. For $0 < S < 1.6$ (regime I), no difference is observed between all values of χ_{CV} , whereas for $1.6 < S < 2$ (regime II) the behaviour of $W(r = 0)$ for $\chi_{CV} = 1$ slightly departs from that for $\chi_{CV} > 1$: this is due to the occurrence of vortex breakdown in the jet in the case $\chi_{CV} = 1$, that results in an axial deceleration already noticeable at $z = 4.70$.

Figure 2 shows a clear change in behaviour when the swirl number is further increased above $S \approx 2$ (regimes III and IV). This is actually linked to the flow becoming locally *subcritical*. This term refers to the propagation direction of the axisymmetric inertial (or Kelvin) waves, which stem from the Coriolis force and are known to strongly influence the dynamics of rotating flows. Similarly to the context of compressible or free-surface flow, a flow invariant by translation in the axial direction is termed supercritical if infinitesimal perturbations are only propagated downstream by these waves, and subcritical if both the upstream and the downstream directions are possible. The subcritical regime is moreover characterized by the ability of the flow to sustain infinitesimal *standing* axisymmetric Kelvin waves. The transition between both regimes is driven by the swirl number and occurs at a critical value denoted S_B , and separates low-swirl supercritical flows ($S < S_B$) from high-swirl number flows ($S > S_B$). The notation S_B refers to the study of Benjamin (1962) on the vortex breakdown phenomenon, which was among the first to highlight such concepts in the framework of rotating flows. In this work, Benjamin described theoretically vortex breakdown as a spatial transition zone between an upstream supercritical flow and a downstream subcritical flow. Such a phenomenology has been confirmed in subsequent experimental (Tsai and Widnall, 1980) and numerical studies (Ruith et al., 2003).

For a flow consisting of a plug axial velocity with solid-body rotation and no boundary layer, it is found that $S_B = j_{1,1}/2 \approx 1.916$, where $j_{1,1}$ denotes the first non-trivial root of the Bessel function of order 1 of the first kind. Interestingly, this value is close to the experimental one ($S \approx 2$).

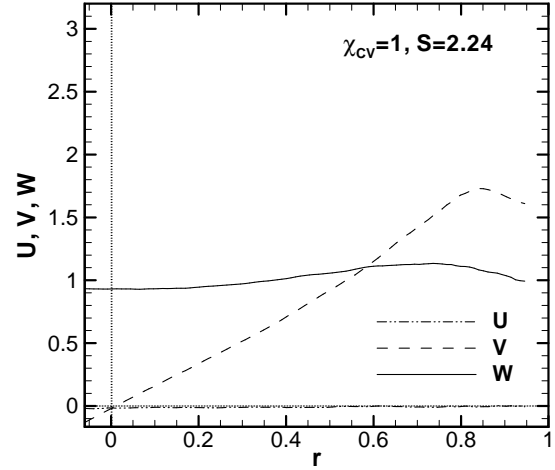


Figure 3: Mean velocity profiles at $z = 4.70$ for $S = 2.24$ ($\chi_{CV} = 1$). The lower zone of the boundary layer is not included due to a spurious reflexion of the laser sheet.

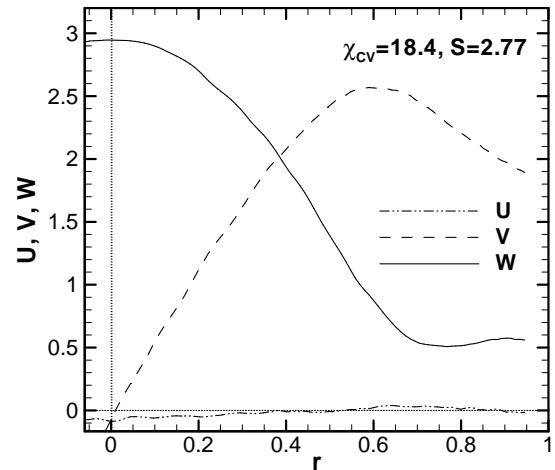


Figure 4: Mean velocity profiles at $z = 4.70$ for $S = 2.77$ ($\chi_{CV} = 18.4$).

For subcritical flows (regimes III and IV), the presence of a contraction downstream leads to a different flow than for $\chi_{CV} = 1$, but the values of $\chi_{CV} > 1$ tested in our study all yield the same dynamics, as seen on figure 2. Whereas for $\chi_{CV} = 1$ profiles with a defect or with an excess of axial velocity on the axis are alternatively found as S is increased, only the latter configuration is obtained for $\chi_{CV} > 1$, with very large values of the velocity excess on the axis (and a corresponding velocity defect at the periphery, i.e. large gradients in the radial direction). Figures 3 and 4 respectively show examples of these velocity profiles, respectively for $\chi_{CV} = 1$, $S = 2.24$ and $\chi_{CV} = 18.4$, $S = 2.77$.

In the case $\chi_{CV} > 1$, the evolution of $W(r = 0)$ with S is explained by the presence in the flow of *large-amplitude* standing axisymmetric Kelvin waves without any breakdown-like phenomenon. This conclusion was confirmed by simulating numerically the flow from the honeycomb to

the jet exit plane for $\chi_{CV} = 4$. We imposed a no-slip condition at the wall, and an inflow condition of solid-body rotation with angular velocity Ω_0 and plug axial flow of velocity W_0 . Steady flow solutions were then sought for a moderate inflow Reynolds number ($Re_0 = R_0 W_0 / \nu = 1000$) and increasing values of the inflow swirl number $S_0 = R_0 \Omega_0 / W_0$ (see Leclaire (2006) for more details on this simulation). Figure 5 displays the axial velocity at $r = 0$ as a function of z obtained for selected values of S_0 . By extracting the value of $W(r = 0)$ at $z = 4.70$, it can be shown that this simulation is in very good agreement with the experimental data even if the Reynolds number are not of same order of magnitude. Figure 5 shows that these waves have a wavelength of order unity, that progressively decreases as S increases, thereby leading to “oscillations” of $W(r = 0)$ when observed at a fixed axial location for increasing S .

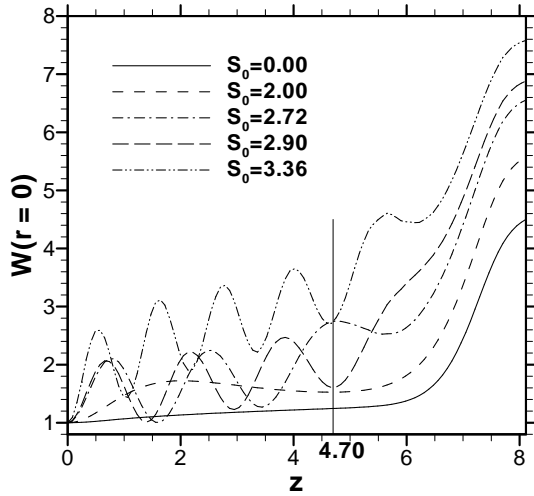


Figure 5: Axial velocity W on the duct axis for different values of S_0 (numerical simulation at $Re_0 = 1000$, $\chi_{CV} = 4$).

The distinction between regimes III and IV is based on the unsteadiness observed in the flow corresponding to $\chi_{CV} > 1$ and will be accounted for in the following.

UNSTEADINESS AND TURBULENCE

To characterize the unsteady and turbulent behaviour of the flow, we first introduce the turbulence rates, built from the mean axial velocity \overline{W} :

$$q_r = \frac{u'}{\overline{W}}, \quad q_\theta = \frac{v'}{\overline{W}}, \quad q_z = \frac{w'}{\overline{W}} \quad (3a)$$

$$q = \sqrt{\frac{\langle u'^2 \rangle + \langle v'^2 \rangle + \langle w'^2 \rangle}{2\overline{W}^2}} \quad (3b)$$

These quantities are here more used as a qualitative way to describe the unsteady flow behaviour, since the number of samples taken at each measurement is not large enough to allow a rigorous convergence of the turbulent quantities.

Conclusions pertaining to the azimuthal symmetry of the perturbations may be drawn from the behaviour of q_θ and q_z at the duct axis. To show this, let us consider infinitesimal normal-mode perturbations

$$(u, v, w)(r, \theta, z, t) = (V, W) + \varepsilon \Re\{(u', v', w')e^{i(kz + m\theta - \omega t)}\}, \quad \text{with } \varepsilon \ll 1 \quad (4)$$

of respective real axial and azimuthal wavenumbers k and m , and complex frequency ω , superimposed on a parallel flow $V(r), W(r)$ (i.e. with no axial gradients nor radial velocity). Upon using a Taylor expansion at $r = 0$, it can be found that for axisymmetric modes ($m = 0$)

$$u'(r), v'(r) = O(r), \quad w'(r), p'(r) = O(1) \quad (5)$$

whereas for asymmetric modes ($m \neq 0$)

$$u'(r), v'(r) = O(r^{|m|-1}), \quad w'(r), p'(r) = O(r^{|m|}) \quad (6)$$

Therefore, $q_\theta(r = 0) \neq 0$ is the signature of a *helical* ($|m| = 1$) perturbation whereas $q_z(r = 0) \neq 0$ is that of an *axisymmetric* ($m = 0$) perturbation.

The $\chi_{CV} = 1$ case

Figure 6 shows the evolution with S of the azimuthal and axial turbulence rates at the centre of the duct for $\chi_{CV} = 1$. An increase of $q_\theta(r = 0)$ is detected from $S \geq 2.24$, revealing the appearance of a helical perturbation. As mentioned above, the flow is found subcritical from $S > 2$ and for certain values of S , axial velocity profiles display a defect on the axis when $\chi_{CV} = 1$. These features are currently encountered in flows downstream of vortex breakdown (see for instance the review of Leibovich, 1984), and could therefore suggest that breakdown occurs upstream from the PIV zone, presumably directly downstream of the honeycomb.

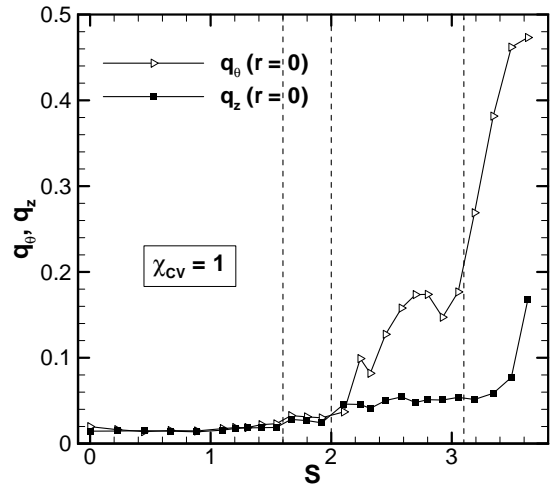


Figure 6: Azimuthal and axial turbulence rates q_θ and q_z at $r = 0$, $z = 4.70$, as a function of S ($\chi_{CV} = 1$).

Figure 7 further characterizes this helical disturbance by plotting the correlation coefficient of the radial velocity fluctuations at $r = 0$, defined by

$$R_{uu}(0, r) = \frac{\langle u'(0)u'(r) \rangle}{\langle u'^2(0) \rangle^{1/2} \langle u'^2(r) \rangle^{1/2}} \quad (7)$$

As soon as this helical instability appears in the flow (i.e. from $S \geq 2.24$), it affects a large central zone of the flow, ranging typically from $r = 0$ to $r = 0.6$. This behaviour is probably to be associated with the significant width of the rotational core in our flow, that actually extends to the boundary layer in a situation with no significant perturbation such as in regimes I and II.

Figure 6 also shows an increase of the axial turbulence rate q_z from $S \geq 3.49$, which indicates the appearance of an axisymmetric perturbation in addition to the helical one.

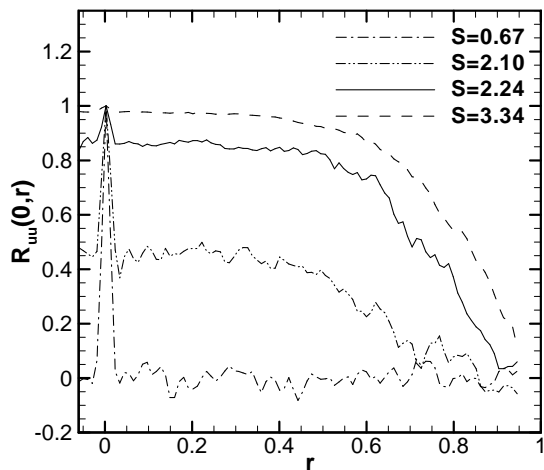


Figure 7: Values of the correlation coefficient of the radial fluctuation $R_{uu}(0, r)$ at $z = 4.70$, for selected values of S ($\chi_{CV} = 1$).

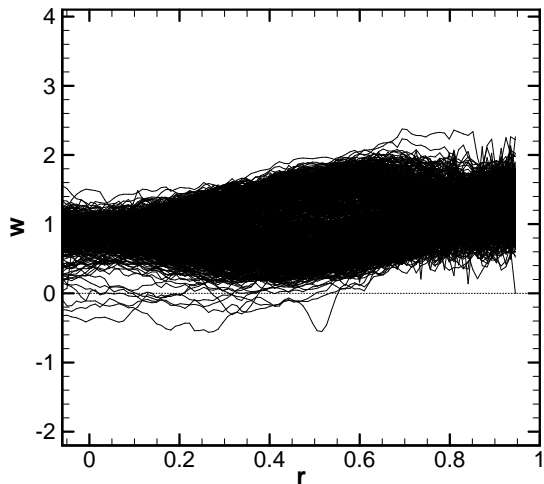


Figure 8: Superposition of instantaneous velocity profiles of the axial velocity w at $r = 0$, $z = 4.70$, for $S = 3.63$ ($\chi_{CV} = 1$).

As a result, for $S = 3.63$, even if the mean axial velocity is strictly positive, transient recirculations close to the duct axis are observed, as plotted on figure 8.

The $\chi_{CV} > 1$ case

As well as for the mean flow, discrepancies between cases $\chi_{CV} = 1$ and $\chi_{CV} > 1$ are observed in the unsteady flow behaviour. Figure 9 plots radial profiles of the total turbulence rate q as a function of the swirl parameter S , for $\chi_{CV} = 18.4$. This particular value of the contraction ratio will be taken in the following as representative of the case $\chi_{CV} > 1$.

As mentioned above, two subcritical flow regimes can be distinguished. In regime III ($2 < S < 3.1$), the turbulence rate remains weak at the duct axis, but progressively increases at the flow periphery. For $2.7 < S < 3.1$ a local maximum of q is observed in the region $r \approx 0.5 - 0.6$. It should be reminded here that this region is not part of the boundary layer nor close to its edge (the boundary layer typically extends from $r = 0.9 - 0.95$ to $r = 1$ in our flow).

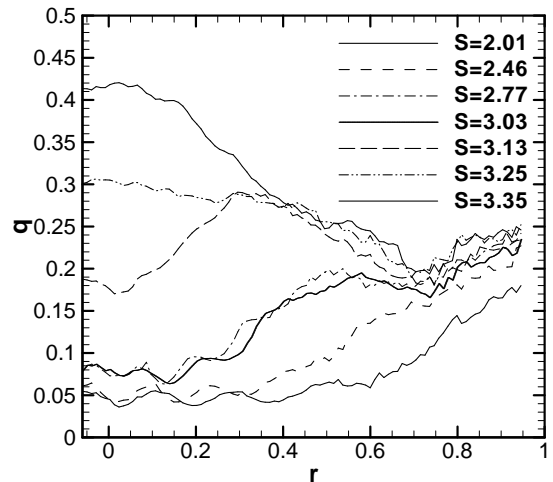


Figure 9: Radial profiles of the total turbulence rate q at $z = 4.70$ as a function of S ($\chi_{CV} = 18.4$).

At $S \approx 3.1$ perturbations of very large amplitude appear at the duct axis. This event is used to define the onset of regime IV. In a similar way to figure 6, figure 10 represents the axial and azimuthal turbulence rates at $r = 0$, together with the total turbulence rate at $r = 0.6$ as a function of S , for $\chi_{CV} = 18.4$. It shows that the perturbations in regime IV are both axisymmetric and helical in nature (the latter being of largest amplitude).

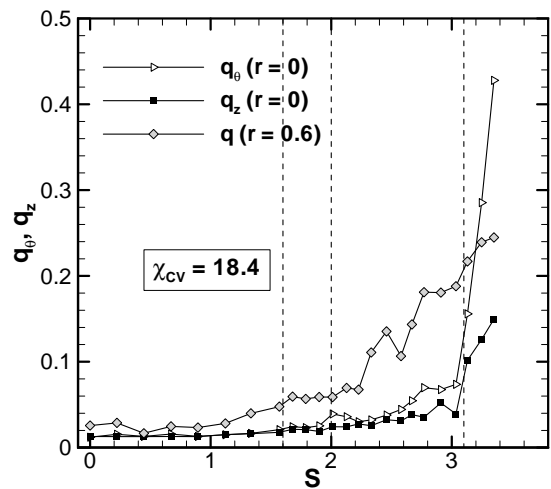


Figure 10: Turbulence rates q_θ and q_z at $r = 0$ and q at $r = 0.6$, $z = 4.70$, as a function of S ($\chi_{CV} = 18.4$).

As an attempt to find the origin of the turbulence in the periphery of the flow in regime III, we applied local instability criteria to the mean flow profiles at $z = 4.70$. It was found that the observed unsteadiness cannot be linked to azimuthal shear, by virtue of the Rayleigh inflexion point criterion applied to the azimuthal component of velocity. Axial shear may be involved since all flows of regime III satisfy the necessary condition of Batchelor and Gill (1962). However this criterion pertains to flows with no azimuthal velocity, therefore a proof of the implication of such a mechanism would require a complete local stability analysis which is out of the scope of the present study. On the contrary, the *sufficient* criterion derived by Leibovich and Stewartson (1983) can be tested here with no further assumption than parallel flow. Though this hypothesis is clearly not

fulfilled in the experiment since standing waves are present in the axial direction, it can be argued that the gradients associated with these standing waves are of the order of magnitude of the duct radius, whereas the criterion of Leibovich and Stewartson (1983) predicts the ability of a parallel flow to undergo a generalized centrifugal instability of *asymptotically small scale*. As a matter of fact, it states that in the limit of infinite $|m|$, the growth rate $\omega_{i\infty}$ of a perturbation superimposed on the base flow $(V(r), W(r))$ satisfies

$$\omega_{i\infty}^2 = \frac{2V(rV_r - V) \left(\frac{V}{r}\right)^2 - V_r^2 - W_r^2}{(rV_r - V)^2 + r^2W_r^2} \quad (8)$$

Generalized centrifugal instabilities indeed seem to be at work in the duct flow, as attested by figures 11 and 12. On the former, radial profiles of q and of $\omega_{i\infty}^2$ are plotted for $S = 2.77$, and are in good agreement, the radial maxima of both quantities nearly coinciding close to $r \approx 0.5$. Figure 12 plots the evolution with S of $\omega_{i\infty, max}^2$, defined as the radial maximum of $\omega_{i\infty}^2$, together with $W(r = 0)$ and $q(r = 0.6)$, still at $z = 4.70$. Here, it is useful to remind that the value of $W(r = 0)$ can be used as an evaluation of the magnitude of the flow gradients in the radial direction. Therefore, figure 12 shows that the value of $\omega_{i\infty, max}^2$ strongly depends on the magnitude of these gradients. Moreover, the increase of $q(r = 0.6)$ also seems to correlate well with the evolution of $\omega_{i\infty, max}^2$, thereby confirming the implication of generalized centrifugal instabilities of small scale to explain the turbulence at the flow periphery.

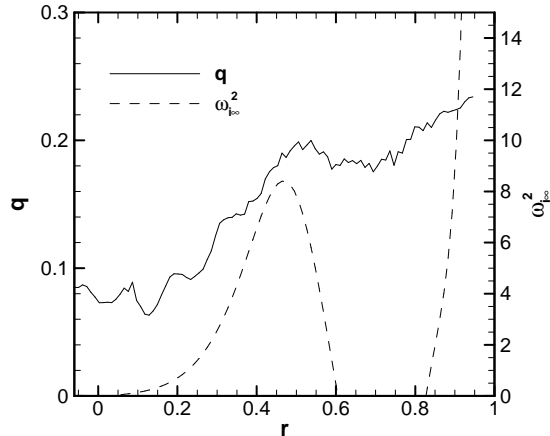


Figure 11: Comparison of the radial profiles of q and of the value of the growth rate $\omega_{i\infty}^2$ yielded by the criterion of Leibovich and Stewartson (8) at $z = 4.70$ for $S = 2.77$ ($\chi_{CV} = 18.4$).

Contrary to the case $\chi_{CV} = 1$, axial and azimuthal perturbations set on at the same value of the swirl number $S \approx 3.1$. Even if their respective orders of magnitude are comparable to the case $\chi_{CV} = 1$ (see figure 6), the helical perturbation is characterized by a smaller radial coherence length scale. This is shown in figure 13, which plots $R_{uu}(0, r)$ for different swirl numbers of regime IV in the case $\chi_{CV} = 18.4$. As a matter of fact, for $S = 3.13$ and 3.25 , $R_{uu}(0, r)$ is seen to decrease steeply for $r > 0$, and it is only for the highest swirl value $S = 3.35$ that more radial coherence is attained, $R_{uu}(0, r)$ decreasing less steeply for $0 < r < 0.45$ than for larger r .

More striking is the superposition of radial profiles of the axial velocity W for $S = 3.35$, plotted in figure 14. Consistently with the presence of a large velocity excess on the

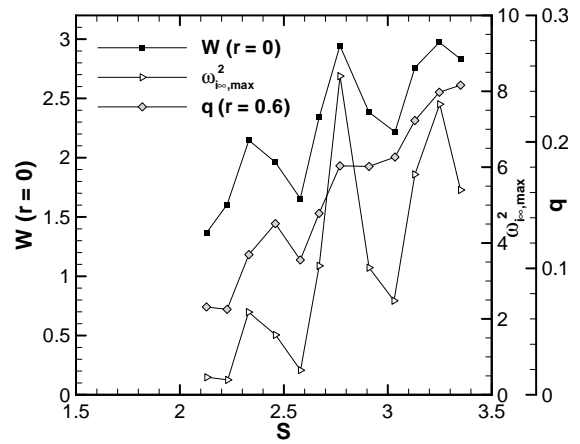


Figure 12: Evolution with S of the mean axial velocity W at $r = 0$, together with the mean turbulence rate q at $r = 0.6$ and the maximum of $\omega_{i\infty}^2$ over a radial profile at $z = 4.70$, for $\chi_{CV} = 18.4$.

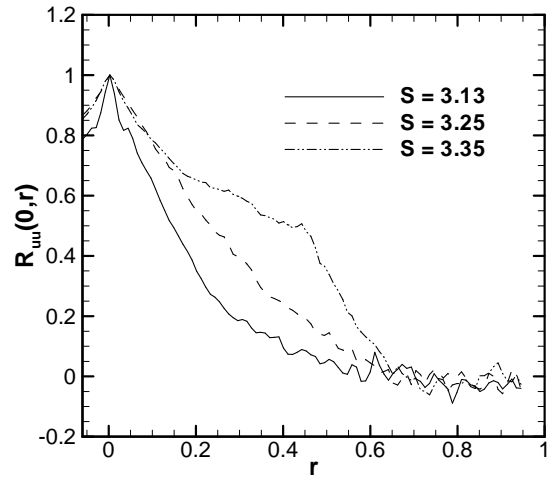


Figure 13: Values of the correlation coefficient of the radial fluctuation $R_{uu}(0, r)$ at $z = 4.70$, for selected values of S ($\chi_{CV} = 18.4$).

duct axis, a minimum of W is observed at the flow periphery (between $r = 0.7$ and $r = 0.8$). As a consequence of the axisymmetric instability, transient small-scale recirculations are observed in that zone. Such events are the counterpart of the recirculations illustrated in figure 8 for $\chi_{CV} = 1$, which occur in that case near the duct axis due to the different mean velocity profiles.

CONCLUSION

In this paper we investigated the duct flow upstream of a high-Reynolds-number swirling jet with a large zone of solid-body rotation. We measured by Stereo-PIV the flow in a duct portion located directly upstream of the final contraction that generates the jet, and also considered the case where this contraction is replaced by a straight duct. We studied the parametric influence of the swirl number S of the flow generated by the honeycomb and of the contraction ratio χ_{CV} of the final duct portion. It has been found that supercritical flows have a simple dynamics and remain weakly unsteady or turbulent, and that subcritical duct flows are on the contrary characterized by a complex mean flow

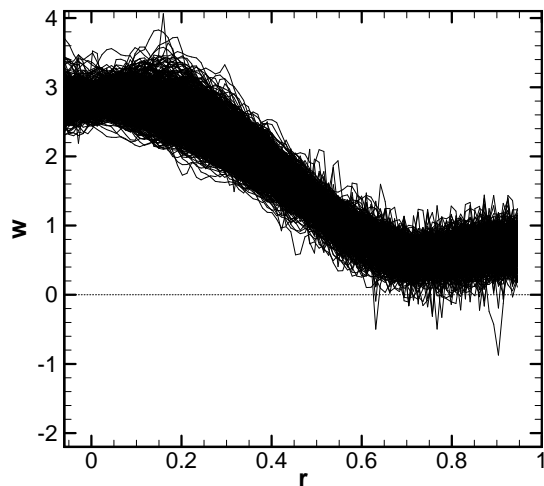


Figure 14: Superposition of instantaneous velocity profiles of the axial velocity w at $r = 0$, $z = 4.70$, for $S = 3.35$ ($\chi_{CV} = 18.4$).

structure and important unsteadiness. Subcritical flows are moreover strongly influenced by the geometry of the downstream duct since large discrepancies have been observed between the flows corresponding to $\chi_{CV} = 1$ and $\chi_{CV} > 1$. However no difference has been noted between $\chi_{CV} = 4, 9$ and 18.4 . In the cases $\chi_{CV} > 1$, the mean flow displays large-amplitude standing axisymmetric Kelvin waves, which may result in important radial velocity gradients in the flow, with a large axial velocity excess on the axis and low axial velocity close to the boundary layer. When $\chi_{CV} = 1$, these gradients are weaker or of opposite sign (i.e. the axial velocity profiles may display a velocity defect on the axis).

The unsteady behaviours differ as a result of these discrepancies in the mean flow. In the case $\chi_{CV} = 1$, a helical perturbation with a large radial coherent scale is observed from the beginning of regime III, followed by an axisymmetric perturbation in regime IV, which leads to transient recirculations near the duct axis. In the case $\chi_{CV} > 1$, no significant helical or axisymmetric perturbation are observed in regime III, but small-scale generalized centrifugal instabilities lead to a production of turbulence in the periphery of the flow. A helical and an axisymmetric perturbation appear simultaneously in regime IV, the former being characterized by a smaller radial coherence length scale than for $\chi_{CV} = 1$, and the latter leading to transient small-scale recirculations in the flow periphery, close to the boundary layer edge.

To this day, the origin of these helical and axisymmetric perturbations remains unclear and therefore deserves further theoretical and numerical studies. Work is in progress along these lines.

REFERENCES

- Batchelor, G. K., Gill, A. E., 1962, "Analysis of the stability of axisymmetric jets," *J. Fluid Mech.*, Vol. 14, pp. 593-629.
- Benjamin, T. B., 1962, "Theory of the vortex breakdown phenomenon," *J. Fluid Mech.*, Vol. 14, pp. 593-629.
- Billant, P., Chomaz, J-M., Huerre, P., 1998, "Experimental study of vortex breakdown in swirling jets," *J. Fluid Mech.*, Vol. 376, pp. 183-219.
- Leclaire, B., 2006, "Etude thorique et experimentale d'un coulement tournant dans une conduite", Ph.D. Thesis, Ecole

Polytechnique, Palaiseau, France.

Leibovich, S., Stewartson, K., 1983, "A sufficient condition for the instability of columnar vortices," *J. Fluid Mech.*, Vol. 126, pp. 335-356.

Leibovich, S., 1984, "Vortex stability and breakdown: survey and extension," *AIAA J.*, Vol. 22(9), pp. 1192-1206.

Lucca-Negro, O., O'Doherty, T., 2001, "Vortex breakdown: a review," *Prog. Energy Combust. Sci.*, Vol. 27, pp. 431-481.

Panda, J., McLaughlin, D. K., 1994, "Experiments on the instabilities of a swirling jet," *Phys. Fluids*, Vol. 6(1), pp. 263-276.

Ruith, M. R., Chen, P., Meiburg, E., Maxworthy, T., 2003, "Three-dimensional vortex breakdown in swirling jets and wakes: direct numerical simulation," *J. Fluid Mech.*, Vol. 486, pp. 331-378.

Tsai, C., Widnall, S. E., 1980, "Examination of group-velocity criterion for breakdown of vortex flow in a divergent duct," *Phys. Fluids*, Vol. 23(5), pp. 864-870.